radiation damage

Specific radiation damage to acidic residues and its relation to their chemical and structural environment

Emanuela Fioravanti,[a]*‡ Frédéric M. D. Vellieux,[a] Patricia Amara,[b] Dominique Madern[a] and Martin Weik[a]*

[a]Laboratoire de Biophysique Moléculaire, Institut de Biologie Structurale J.-P. Ebel, CEA CNRS UJF, 41 Rue Jules Horowitz, 38027 Grenoble CEDEX 1, France, and [b]Laboratoire de Dynamique Moléculaire, Institut de Biologie Structurale J.-P. Ebel, CEA CNRS UJF, 41 Rue Jules Horowitz, 38027 Grenoble CEDEX 1, France. E-mail: fioravan@esrf.fr, weik@ibs.fr

Intense synchrotron radiation produces specific structural and chemical damage to crystalline proteins even at 100 K. Carboxyl groups of acidic residues (Glu, Asp) losing their definition is one of the major effects observed. Here, the susceptibilities to X-ray damage of acidic residues in tetrameric malate dehydrogenase from *Haloarcula marismortui* are investigated. The marked excess of acidic residues in this halophilic enzyme makes it an ideal target to determine how specific damage to acidic residues is related to their structural and chemical environment. Four conclusions are drawn. (i) Acidic residues interacting with the side-chains of lysine and arginine residues are less affected by radiation damage than those interacting with serine, threonine and tyrosine side-chains. This suggests that residues with higher pK_a values are more vulnerable to damage than those with a lower pK_a. However, such a correlation was not found when calculated pK_a values were inspected. (ii) Acidic side-chains located in the enzymatic active site are the most radiation-sensitive ones. (iii) Acidic residues in the internal cavity formed by the four monomers and those involved in crystal contacts appear to be particularly susceptible. (iv) No correlation was found between radiation susceptibility and solvent accessibility.

Keywords: radiation damage; acidic residues; halophilic malate dehydrogenase.

1. Introduction

Ionizing radiation, including that generated by synchrotron sources, has specific effects on the activity, stability and structure of biological macromolecules. Even at cryogenic temperatures, X-ray absorption initiates chemical reactions in crystalline proteins that affect their structures (reviewed by Garman, 2003, and by Carugo & Carugo, 2005). Radiation damage can be an important limitation to the success of crystallographic experiments at third-generation synchrotron sources. During the past few years an increasing number of experiments have been performed in order to better understand the effect of ionizing radiation on protein crystals. In this context, synchrotron radiation represents both the cause of damage and the tool to study it.

Specific radiation damage includes breakage of disulfide bonds and loss of definition of the carboxyl group of acidic residues (Burmeister, 2000; Ravelli & McSweeney, 2000; Weik *et al.*, 2000). The latter has been attributed to decarboxylation,

yet definitive experimental confirmation is still missing. Residues in active sites have repeatedly been reported to be highly radiation-sensitive (Burmeister, 2000; Ravelli & McSweeney, 2000; Weik *et al.*, 2000, 2001; Matsui *et al.*, 2002; Adam *et al.*, 2004; Baxter *et al.*, 2004; Dubnovitsky *et al.*, 2005; Roberts *et al.*, 2005; Leiros *et al.*, 2006). Radiation damage to acidic residues is a secondary effect and its extent varies from residue to residue within the protein crystal under investigation. It remains unclear, however, which factors influence most the extent of specific damage. In previous radiation-damage studies on mesophilic proteins, the low number of acidic residues was a limiting factor to a detailed analysis. Here we investigate specific radiation damage to the halophilic protein malate dehydrogenase from *Haloarcula marismortui* (*Hm* MalDH), an enzyme that contains twice as many acidic residues as mesophilic proteins.

Halophilic *Archaea* grow optimally in molar NaCl. They balance the external high salt concentration by accumulating intracellular KCl. Stable, soluble and active in high salt concentrations, proteins purified from these organisms show a peculiar amino acid composition (Madern *et al.*, 2000;

Table 1
Photon flux and absorbed dose for each data set and burn.

	Data set 1	Burn 1	Data set 2	Burn 2	Data set 3
Flux (photons s^{-1})	1.359×10^{11}	33.25×10^{11}	1.558×10^{11}	33.54×10^{11}	1.558×10^{11}
Absorbed dose (Gy)	1.2×10^6	2.0×10^6	1.4×10^6	2.1×10^6	1.5×10^6

Mevarech et al., 2000) with an enrichment of acidic residues (Yamada et al., 2002). Indeed, 20% of all residues in Hm MalDH are acidic ones. They are located mostly on the surface where they interact with water molecules and salt ions, and are involved in a large number of salt bridges that stabilize the enzyme (Dym et al., 1995; Richard et al., 2000; Irimia et al., 2003).

Hm MalDH, a homotetramer of 130 kDa with 303 residues per monomer (Richard et al., 2000), is an enzyme involved in the citric acid cycle where it catalyses the oxidation of malate to oxaloacetate with the concomitant reduction of NAD$^+$ to NADH. Hm MalDH belongs to the tetrameric (lactate dehydrogenase-like) group of MalDH (for a review, see Madern, 2002), a group of enzymes closely related to lactate dehydrogenases (LDH). Crystallographic structures of (LDH-like) MalDH orthologs have demonstrated that they share the same fold with LDHs (Irimia et al., 2004; Dalhus et al., 2002; Lee et al., 2001). Substrate discrimination between LDH and (LDH-like) MalDH is due to a single amino acid substitution at position 102 on the mobile catalytic loop (residues 100 to 107) (Madern, 2002). Observations obtained from structural studies of LDHs are thus completely valid for Hm MalDH.

In the present work, radiation susceptibilities of acidic side-chains of Hm MalDH were analysed with respect to their location in the three-dimensional structure, their chemical environment, their calculated pK_a value and their solvent accessibility.

2. Materials and methods

2.1. Expression, purification and crystallization

Hm MalDH was expressed in E. coli BL21 (DE3). Protein purification and removal of the NADH cofactor was carried out as described previously (Cendrin et al., 1993; Madern et al., 1995). The protein was concentrated to 50 mg ml^{-1} and stored in 20 mM phosphate buffer (Na$_2$HPO$_4$), pH 7.0, 4 M NaCl, at 277 K. Crystals of the apo-enzyme were obtained at room temperature by the sitting-drop reverse vapor diffusion method, using the ternary NaCl:2-methyl-2,4-pentanediol-(MPD):H$_2$O system (Richard et al., 1995; Costenaro et al., 2001). 3 μl of protein solution and 4 μl of MPD were equilibrated against 1 ml reservoirs containing 58% (v/v) MPD in water.

2.2. Data collection and dose calculation

All data were collected on the ESRF beamline ID23-EH1 at an energy of 13.2 keV (λ = 0.939 Å). The photon flux (Table 1) was determined after calibrating the beamline diodes against a reference photodiode with known photon flux characteristics (Ravelli & McSweeney, 2000).

A crystal of apo Hm MalDH (200 μm × 200 μm × 200 μm in dimension) was loop-mounted and flash-cooled to 100 K. Three data sets were collected, intercalated by two X-ray 'burns' (data set 1, burn 1, data set 2, burn 2, data set 3) using a beam with a size of 100 μm × 100 μm. The data sets (180 frames of 1° rotation, 1 s per frame exposure times) were collected using an attenuated beam (5% transmission). During the 'burns', the crystal was rotated around the same angular range, while being exposed for 12 s to the unattenuated beam (100% transmission). No translation along the spindle axis was applied during data collection and burns.

The absorbed X-ray doses (Tables 1 and 2) were estimated using RADDOSE (Murray et al., 2004, 2005), based on crystal and X-ray beam sizes and shapes, photon flux and energy and crystal absorption and density, which were calculated from unit-cell content and known crystallization conditions. The total accumulated dose after collection of data set 3 was 8.2×10^6 Gy, corresponding to about half of the Henderson limit (2×10^7 Gy; Henderson, 1990) and a third of the Garman limit (3×10^7 Gy; Owen et al., 2006).

2.3. Data reduction and structure refinement

All data sets were integrated using MOSFLM (Leslie, 1992) and further processed using the CCP4 programs SCALA and TRUNCATE (Collaborative Computational Project, Number 4, 1994). The crystal belongs to space group C_2 with unit-cell dimensions as indicated in Table 2. The asymmetric unit contains a tetramer with a solvent content of 63% (v/v).

The structure of the (R207S, R292S) double mutant of Hm MalDH [Protein Data Bank (PDB) code 1o6z; Irimia et al., 2003] was used as the starting point for model building. The Hm MalDH model corresponding to data set 1 (model 1) was refined using CNS (Brünger et al., 1998), using bulk solvent correction and a maximum-likelihood target function. Rigid-body refinement was followed by cycles of simulated annealing, conjugate gradient minimization, individual isotropic temperature factor (B-factor) refinement and model building using O (Jones et al., 1991). Side-chain atoms without electron density appearing at the 1.0σ level in $3mF_o - 2DF_c$ maps were removed from the model. Residues in position 100–107, corresponding to the mobile catalytic loop, were excluded from the model of monomers B and D because of their poor electron density. The same residues are well defined in monomers A and C, since they are held in place by crystal contacts with symmetry-related molecules. Models 2 and 3 were obtained by refining the reference model 1 (including its water and ion components) versus data sets 2 and 3, respectively. The procedure consisted of rigid-body refinement

Table 2
Data processing and structure refinement statistics.

Numbers in parentheses refer to the highest-resolution shell. R.m.s.d. = root-mean-square deviation.

Data set	1	2	3
Accumulated absorbed dose (Gy)	1.2×10^6	4.6×10^6	8.2×10^6
Resolution (Å)	20−2.0 (2.11−2.0)	20−2.15 (2.27−2.15)	20−2.25 (2.37−2.25)
Unit-cell parameters (Å)			
a	127.15	126.98	127.38
b	114.24	114.32	114.57
c	124.14	124.12	124.53
R_{sym} (%)†	10.1 (30.5)	10.2 (28.1)	10.8 (33.2)
Mean ($\langle I/\sigma_I \rangle$)	11.1 (3.0)	11.4 (3.4)	11.1 (3.0)
Multiplicity	3.2 (3.2)	3.3 (3.1)	3.3 (3.2)
Completeness (%)	93.9 (85.4)	95.5 (89.2)	96.2 (90.8)
Unique reflections	112033 (14865)	91779 (12484)	81346 (11144)
Observations/parameters ratio	2.8	2.3	2.0
R_{cryst}‡ (R_{free}§) (%)	22.5 (27.0)	22.0 (26.7)	22.0 (27.1)
R.m.s.d. bonds (Å)	0.012	0.011	0.010
R.m.s.d. angles (°)	1.53	1.49	1.43
Average isotropic temperature factor (Å^2)	21.3	22.0	24.3

† $R_{sym} = \Sigma |I_{obs} - \langle I \rangle| / \Sigma \langle I \rangle$. ‡ $R_{cryst} = \Sigma |F_{obs} - F_{calc}| / \Sigma F_{obs}$. § R_{free} was calculated with a small fraction (5%) of randomly selected reflections (the same indices were flagged in data sets 1, 2 and 3).

followed by cycles of simulated annealing, conjugate gradient minimization and individual isotropic temperature factor refinement. The quality of the models was assessed using *PROCHECK* (Laskowski *et al.*, 1993) and *WHATCHECK* (Vriend, 1990). Refinement statistics and geometry analysis of the three structures are summarized in Table 2. Figs. 1–4 were prepared using *PyMOL* (DeLano, 2003).

2.4. Radiation damage quantification and analysis of the chemical environment

In order to visualize the specific radiation damage affecting acidic residues and its progression with the accumulated dose, difference Fourier maps were calculated between data sets 2 and 1 and between data sets 3 and 1, using phases from model 1. The structure-factor amplitudes of data sets 2 and 3 were scaled to those of data set 1 (using single scale and isotropic B-factors).[1] The difference Fourier maps were computed to 2.15 ($F_o^2 - F_o^1$) and 2.25 Å ($F_o^3 - F_o^1$) resolution, using the unit-cell parameters of data set 1. The height of peaks [h, expressed in standard deviations (σ) above the mean value (zero) of the difference density map] on carboxyl groups of acidic residues were compared and the degree of damage classified as follows: *high* ($h < -5.5\sigma$), *medium* ($-5.5\sigma < h < -4.5\sigma$), *low* ($-4.5\sigma < h < -3.0\sigma$) and *absent* ($h > -3.0\sigma$). All acidic residues included in the analysis are listed in Table 3, starting with the most damaged side-chains located in the $F_o^3 - F_o^1$ difference Fourier map. The acidic residues whose side-chain B-factors (calculated using the program *BPLOT*; Collaborative Computational Project, Number 4, 1994) in model 1 refined to values exceeding 120% of the average overall B-factor in model 1 (29 out of 61) were considered to be too disordered and were not included in the analysis. The 32 acidic residues that were analysed partitioned equally between the surface

and the interior of the protein. Seven are extremely accessible to the solvent (accessibility > 70 Å^2) and six are buried (accessibility < 20 Å^2). On the other hand, almost all the residues excluded from the analysis are extremely accessible to the solvent (accessibility > 70 Å^2 for 26 out of 29). The environment of the acidic side-chains was analysed both using *DISTANG* (Collaborative Computational Project, Number 4, 1994) and visually using *O* (Jones *et al.*, 1991); all interactions shorter than 3.2 Å are listed in the supplementary material.[2] A calculation of the solvent accessibility of each residue was performed using the program *STRIDE* (Heinig & Frishman, 2004).

2.5. pK_a calculation

The pK_a calculations were performed using an algorithm (M. J. Field, P. Amara, L. David & D. Rinaldo, unpublished results) that implements a method based on the Poisson–Boltzmann approach (Gilson, 1993; Antosiewicz *et al.*, 1994). With this method, the initial pK_a of each titrable residue (experimental value for the residue isolated in solution) is corrected to account for the effects of desolvation and coulombic interactions with the rest of the protein. Calculations were performed using the X-ray structure of model 1 with the default protonation sites for carboxylic acids. In addition, histidines were protonated on Nδ1 and pK_a was calculated on Nε2. Calculations were carried out at 293 K, using a dielectric constant of 20 and 80 for the protein and the solvent, respectively (Antosiewicz *et al.*, 1994). Atomic charges and radii were taken from the literature (Antosiewicz *et al.*, 1994) except for the H atoms whose effect was included in the corresponding heavy atoms. In order to be consistent with the experimental conditions, we used an ionic strength of 1700 mM.

---

[1] The coordinates and structure factor amplitudes of data sets 1, 2 and 3 have been deposited in the Protein Data Bank under accession codes 2j5k, 2j5q and 2j5r, respectively, and will be released upon publication.

[2] Supplementary data for this paper are available from the IUCr electronic archives (Reference: XH5009). Services for accessing these data are described at the back of the journal.

Table 3
Extent of damage (peak height in the $F_o^3 - F_o^1$ difference Fourier map on the carboxyl group of acidic residues), solvent accessibility and calculated pK_a values for 32 acidic residues in *Hm* MalDH.

	Damage (σ)	Solvent accessibility (Å^2)	pK_a
High			
Asp 168	−7.6	12.1	0.3
Asp 73	−6.3	49.9	3.6
Asp 53	−6.2	31.9	3.0
Asp 143	−6.1	3.5	1.5
Asp 47	−5.9	51.4	2.4
Asp 211	−5.9	49.5	3.1
Asp 324	−5.9	103.5	4.0
Asp 44	−5.8	50.6	4.7
Medium			
Asp 92	−5.5	69.6	3.6
Glu 259	−5.2	40.3	3.6
Asp 264	−5.2	54.0	5.3
Glu 276	−5.2	105.9	3.4
Glu 178	−5.1	103.0	4.9
Asp 115	−5.0	75.5	4.7
Asp 128	−5.0	56.1	5.5
Asp 231	−5.0	39.1	4.9
Glu 311	−4.6	0.0	7.4
Glu 267	−4.6	56.3	3.8
Low			
Glu 304	−4.4	103.6	4.7
Glu 299	−4.4	60.0	4.7
Asp 308	−4.3	55.8	3.4
Glu 278	−4.1	26.7	4.2
Glu 247	−3.7	25.3	3.3
Asp 209	−3.7	15.9	2.4
Asp 87	−3.7	60.1	3.1
Asp 238	−3.4	26.5	3.5
Asp 197	−3.2	144.5	3.4
Glu 194	−3.2	1.1	0.7
Absent			
Glu 224		98.2	5.0
Glu 188		65.7	2.3
Asp 65		0.0	−1.1
Glu 151		65.4	2.4

3. Results and discussion

Radiation-induced structural changes appear in the $F_o^3 - F_o^1$ difference Fourier map as negative peaks (Fig. 1). The highest peaks are all located on carboxyl groups of acidic residues. Note that *Hm* MalDH does not contain disulfide bonds. The same sites are affected in the four monomers with only few exceptions (*e.g.* Asp 53 and Asp 115 are damaged only in monomers *A* and *C*). More than 50% of the acidic side-chains analysed are already damaged after the first burn in data set 2 (data not shown), and the same residues are damaged to a higher extent after the second burn in data set 3. More extensive damage is observed in monomers *A* and *C*. Monomer *C* was chosen as the reference monomer for a detailed analysis of radiation damage for two reasons: the entire polypeptide chain could be modeled in the electron density, and the peaks in the $F_o^3 - F_o^1$ difference Fourier map are on average higher in monomer *C* than in monomer *A*. The extent of damage on the acidic side-chains is described as *high*, *medium*, *low* and *absent* according to the height of peaks appearing in the $F_o^3 - F_o^1$ difference Fourier map (as defined in §2). Of the 61 acidic residues in monomer *C*, 32 were analysed (see §2). Among them, eight show *high*, ten show *medium* and ten show *low* damage, whereas four remain undamaged after the two burns (Table 3).

The most sensitive residues are located in the active sites and in the cavity at the center of the tetramer (Fig. 1). In the following, we analyse Table 3 and discuss how specific radiation damage to acidic residues is related to their location in the protein structure, their interactions with neighboring residues, their solvent accessibility and their calculated pK_a value.

3.1. Radiation damage to active-site residues

The catalytic aspartic acid (Asp 168) is the most radiation-sensitive residue (Fig. 1 and Table 3). Its side-chain is hydrogen bonded to the imidazole ring of the catalytic histidine (His 195, Fig. 2). Asp 143, which is hydrogen-bonded to the main chain of His 195 (Fig. 2), is also heavily radiation-affected. His 195 is the only non-acidic residue to be affected by radiation damage (Fig. 3). After the first burn, a negative peak appeared in the $F_o^3 - F_o^1$ map on the imidazole ring (Fig. 3*B*). After the second burn, the negative peak became more important and positive difference density appeared (Fig. 3*C*). The pair of a positive and a negative difference density peak is indicative of a conformational change of His 195 rather than a chemical modification of the side-chain (Dean *et al.*, 1989; Uchida & Kawakishi, 1993). This conformational change could result from the loss of the hydrogen bond with the damaged Asp 168, as was observed for the catalytic histidine in acetylcholinesterase (Weik *et al.*, 2001). His 195 is the only residue hydrogen-bonded to a damaged aspartic or glutamic acid residue that undergoes a conformational change. His 256, for instance, which is hydrogen-bonded to the considerably damaged Glu 267, remains unaffected after the two burns (not shown). Therefore, active sites contain the most radiation-sensitive residues as reported already earlier (Burmeister, 2000; Ravelli & McSweeney, 2000; Weik *et al.*, 2000, 2001; Matsui *et al.*, 2002; Adam *et al.*, 2004; Baxter *et al.*, 2004; Dubnovitsky *et al.*, 2005; Roberts *et al.*, 2005; Leiros *et al.*, 2006).

One might ask if the increased radiation sensitivity of acidic residues in active sites is related to their protonation state. In LDH, the catalytic aspartic acid is thought to be deprotonated (Clarke *et al.*, 1988). Because of the high structural similarity between LDH and *Hm* MalDH (see §1), Asp 168 in *Hm* MalDH is most likely deprotonated (see also pK_a value, Table 3). The same holds true for the most radiation-sensitive residue of bacteriorhodopsin in its ground state, Asp 85, one of the key residues involved in proton pumping (Matsui *et al.*, 2002). On the other hand, the highly radiation-sensitive active-site residues in the photoactive yellow protein (Glu 46; Kort *et al.*, 2004) and in butyrylcholinesterase (Glu 197; J.-Ph. Colletier, personal communication) are protonated. Therefore, the high radiation sensitivity of acidic residues in active sites does not seem to be related to their respective protonation state.
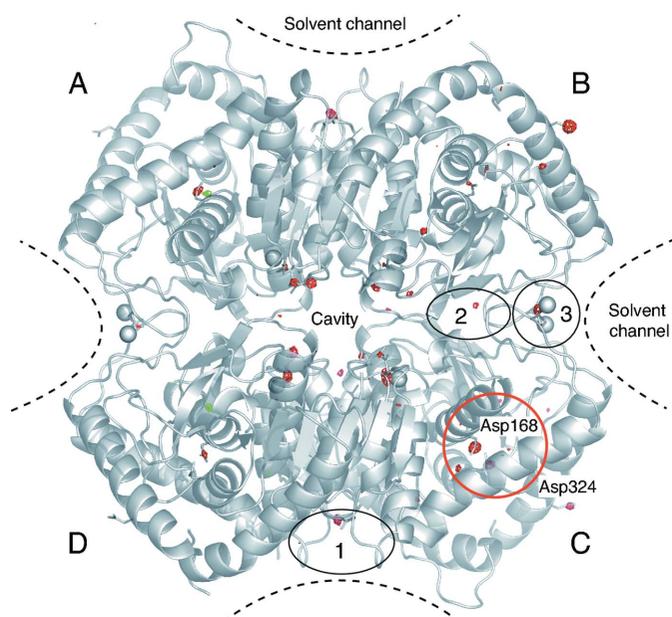
Figure 1
Quaternary structure of *Hm* MalDH in its apo-form and structural changes caused by radiation damage. *Hm* MalDH is a homotetrameric molecule; *A–D* identify the four monomers. The two tight dimers (*A–B*) and (*C–D*) delineate a cavity, filled by a network of over 100 ordered water molecules. Solvent channels are indicated by dashed lines. The regions with salt-bridge clusters (numbered 1–3, as described by Richard *et al.*, 2000) are highlighted. Secondary structures are shown as ribbons, and side-chains of damaged acidic residues as sticks. Eight chloride ions, rendered as spheres, are localized at monomer interfaces. The $F_o^3 - F_o^1$ difference electron density map (negative contours in red and positive contours in green drawn at $\pm 5.0\sigma$ levels) is overlaid on the reference model 1. The active site (red circle, Asp 168) and the cavity display the highest negative peaks which correspond to the loss in electron density associated to the side-chains of the most radiation-damage-sensitive residues (*high* damage, see Table 3).

The observation of enzyme inactivation generally preceding global unfolding led to the suggestion that enzymatic active sites are usually more easily perturbed than the molecule as a whole, and that they are more flexible than the rest of the structure (Tsou, 1998). The flexibility as well as the strained conformation of residues involved in the catalytic reactivity (Dubnovitsky *et al.*, 2005) might be responsible for the increased radiation sensitivity observed for the active site. In *Hm* MalDH the observation of high damage to Asp 53 (Table 3) is in line with this suggestion. This residue is not located in the active site but is involved in the binding of the cofactor NADH by interacting with the ribose hydroxyl groups of its adenosine moiety (Irimia *et al.*, 2003). Studies on LDH have shown that important conformational changes occur during catalysis (Gerstein & Chothia, 1991), involving a transient melting of 10–15% of the protein that is responsible for aligning the NADH molecule in the catalytic site (McClendon *et al.*, 2005). Those structural changes alter the direct environment of the active site (Iwata *et al.*, 1994).

In MalDHs, the His 195–Asp 168 pair has been suggested to function as a proton relay system during catalysis (Birktoft & Banaszak, 1983). Mutation studies have demonstrated that deleting the negative charge on Asp 168 destabilizes the binding of substrate and cofactor to the enzyme (Clarke *et al.*,
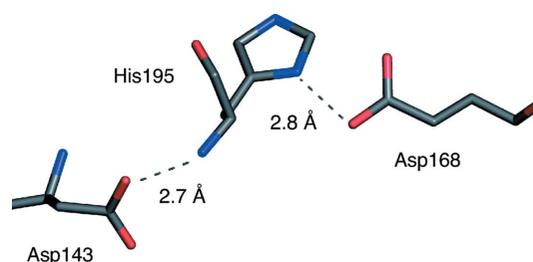
Figure 2
Hydrogen-bond pattern among the active-site residues Asp 168, His 195 and Asp 143.
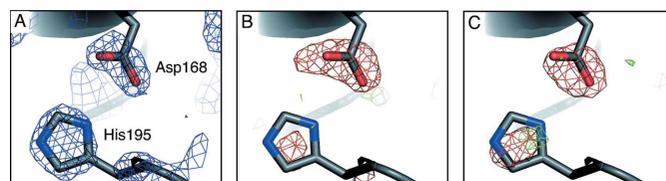
Figure 3
Radiation damage at the active-site residues Asp 168 and His 195. In panel *A*, the $(2F_o - F_c)$ *OMIT* map (in blue) (calculated after simulated annealing, omitting a sphere of 3.5 Å around Asp 168 and His 195) is contoured at the 2.0σ level for the reference model 1. In panels *B* and *C*, the difference electron density maps $F_o^2 - F_o^1$ and $F_o^3 - F_o^1$ (negative contours in red and positive contours in green drawn at $\pm 3.5\sigma$ levels) are overlaid on the reference model 1. The red difference density seen around Asp 168 is indicative of decarboxylation, and the positive and negative difference density peaks on His 195 indicate a conformational change.

1988). Therefore, radiation-induced damage to Asp 168 most likely inactivates the enzyme.

3.2. Radiation damage to surface and cavity residues

Among the most radiation-sensitive residues are the four acidic ones located in the central cavity (Asp 73, Asp 44, Asp 259, Glu 267); two show *high* and two display *medium* damage (Table 3). Among the seven surface residues analysed (Asp 324, Glu 276, Glu 178, Asp 115, Glu 304, Asp 197, Glu 224), only one (Asp 324, Fig. 1) shows *high* damage. It is interesting to compare the damage occurring at the protein surface with that observed at the cavity surface. All residues located within the cavity are radiation-sensitive (*i.e.* they show either *high* or *medium* damage), whereas residues on the surface are not always damaged (Glu 304, Asp 197, Glu 224 show either low or no damage). Asp 324, the only surface residue with high radiation sensitivity, is located in a region involved in crystal contacts and is particularly damaged in monomers *B* and *C* (Fig. 1).

As previously discussed in §2, residues refining to the higher *B*-factor values were not included in our study. This approach guarantees that only highly ordered side-chains are inspected; on the other hand, it excludes almost 50% of the surface residues from the analysis. Despite the limited analysis, our results strongly suggest that residues located on the cavity surface are on average more radiation-sensitive than surface residues. Both the cavity and the crystal channels are solvent
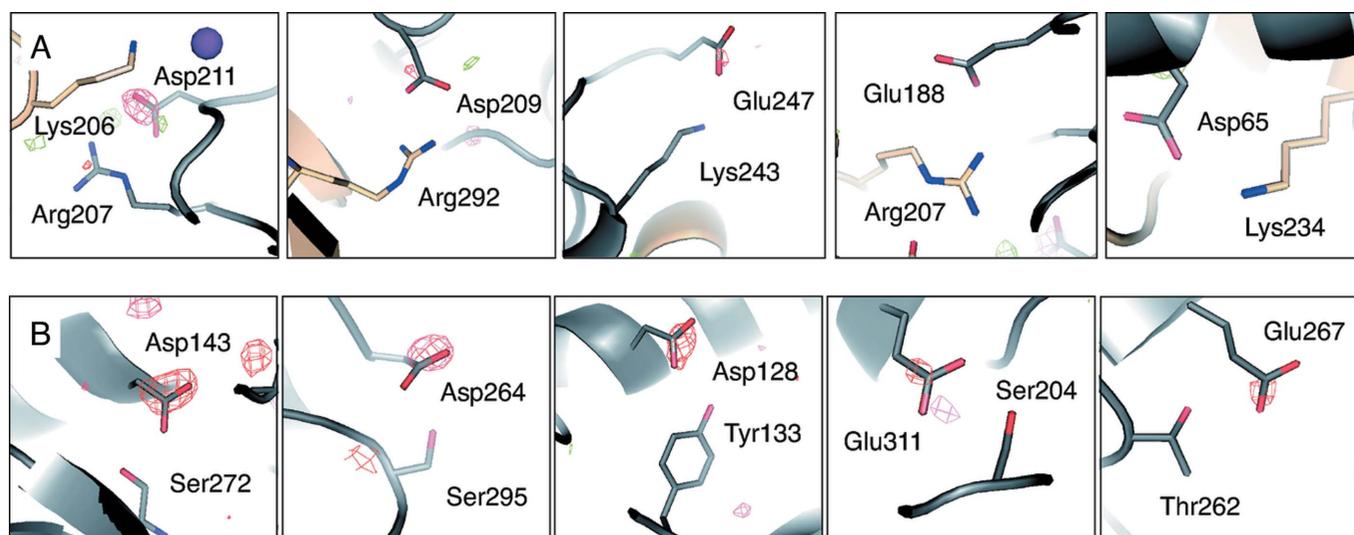
Figure 4
Panel *A* shows the damage occurring at residues involved in the salt-bridge clusters [cluster 1 (Glu 247 and Asp 65), cluster 2 (Asp 209) and cluster 3 (Asp 211 and Glu 188); Richard *et al.*, 2000]. Panel *B* shows the damage of residues involved in interactions with the hydroxyl group of Ser, Tyr or Thr residues. The amino acids are shown as sticks (grey, monomers *A* and *C*; copper, monomers *B* and *D*). The difference electron density maps ($F_o^3 - F_o^1$, negative contours in red and positive contours in green drawn at $\pm 3.5\sigma$) are overlaid on the reference model 1.

reservoirs, yet with different sizes. The cavity is an isolated restricted area (20 Å × 10 Å × 38 Å), whereas the solvent channels are interconnected and wider (diameter 40–50 Å). We can only speculate that the increased radiation sensitivity of the cavity residues is related to the confinement of the solvent in a smaller volume. A possible explanation for this observation remains to be found.

Besides the four residues whose side-chains point towards the center of the cavity (Asp 73, Asp 44, Asp 259, Glu 267), others in the vicinity of the cavity show either *high* or *medium* radiation sensitivity. They are located at the non-crystallographic symmetry contacts between monomers, in particular those between monomers *B* and *D* and between monomers *A* and *C* (Asp 47, Asp 92, Asp 264). Hence, residues located at the non-crystallographic symmetry contacts, as well as the one located at the crystallographic symmetry contacts (Asp 324), appear to be highly radiation-susceptible, as has also been observed in crystalline dodecin (Murray *et al.*, 2005).

3.3. Residues involved in salt bridges are less radiation damaged

In order to relate the chemical environment of acidic residues to their radiation sensitivity, all interactions shorter than 3.2 Å have been listed in the supplementary material. Acidic residues whose side-chains are stabilized by ionic interactions with positively charged residues are on average less damaged than those interacting *via* hydrogen bonds with uncharged residues. In particular, acidic residues involved in salt-bridge clusters 1, 2 and 3 (Figs. 1 and 4*A*; Richard *et al.*, 2000) are less sensitive than those making a hydrogen bond to the hydroxyl group of serine, tyrosine or threonine residues (Fig. 4*B*). All five acidic residues, being hydrogen bonded to either serine, tyrosine or threonine residues, show either *high* or *medium*

damage. Among all the acidic residues in salt-bridge clusters (five), only Asp 211 displays *high* damage, whereas the other four show either *low* or no damage (Table 3, Fig. 4*A*). Indeed, Glu 188 (cluster 3; Figs. 1 and 4*A*) and Asp 65 (cluster 1; Figs. 1 and 4*A*) are completely unaffected by the two X-ray burns. The salt-bridge clusters, conferring stability to *Hm* MalDH under high salt conditions, are probably also important in maintaining the quaternary structure of the crystalline enzyme after irradiation.

3.4. Radiation damage is not related to calculated pK_a values

The observation that acidic residues involved in salt bridges are less radiation-sensitive than those being hydrogen-bonded to serine, tyrosine or threonine residues suggests a relation between radiation damage to acidic side-chains and their pK_a value. However, such a correlation was not found when calculated pK_a values were analysed (Fig. 5), as was also suggested by previous studies involving experimentally
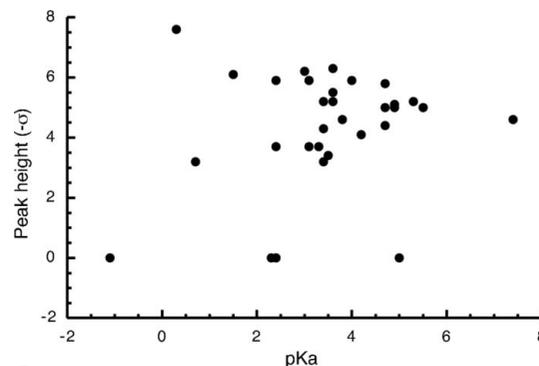
Figure 5
Relationship between radiation damage and calculated pK_a values. The peak heights in the $F_o^3 - F_o^1$ difference Fourier map are plotted as a function of the pK_a value for each residue analysed.
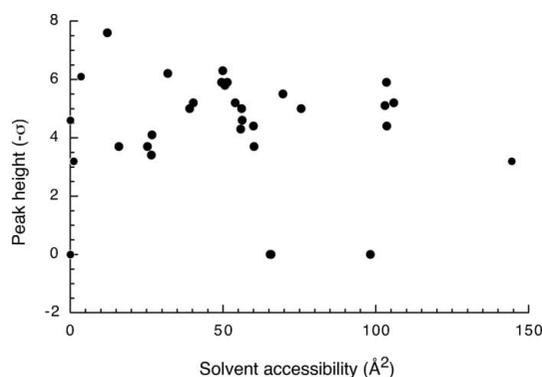
Figure 6
The relation between radiation damage and solvent accessibility. The peak heights in the $F_o^3 - F_o^1$ difference Fourier map are plotted as a function of the solvent accessibility of each residue analysed.

determined pK_a values (Ravelli & McSweeney, 2000). We cannot exclude the fact that the absence of a correlation is due to the fact that pK_a values were calculated at room temperature while the radiation sensitivity of acidic residues was determined at 100 K.

3.5. Radiation damage is not related to solvent accessibility

Analysing the effect of radiation damage on surface residues is fundamental in order to try to establish a correlation between specific radiation damage and solvent accessibility. However, such analysis can be difficult as the side-chains of these residues are often very mobile in crystalline proteins. For this reason, residues with poor electron density and high temperature factor values in the initial model (model 1) have not been considered for this study (see §2). As in previous studies (Ravelli & McSweeney, 2000; Burmeister, 2000), our work did not evidence a correlation between radiation sensitivity and the degree of solvent accessibility of carboxyl groups (Fig. 6). *Hm* MalDH contains highly solvent accessible residues showing either *high* (Asp 324), *medium* (Glu 276, Glu 178), *low* (Asp 197) or even no (Glu 224) damage. Residues with low solvent accessibility, on the other hand, also show *high* (Asp 168, Asp 143), *medium* (Glu 311), *low* (Asp 209, Glu 194) and no (Asp 65) damage.

4. Summary

The relation between the X-ray radiation sensitivity of a large number of acidic residues (32) and their chemical and structural environment was analysed in *Hm* MalDH. The following conclusions emerged:

(i) Acidic residues located in the active site are most radiation sensitive, probably related to the peculiar characteristics of catalytic sites, such as unusual chemical interactions and conformational flexibility.

(ii) Acidic residues on the surface of a cavity formed by monomers of the tetrameric enzyme are more radiation sensitive than those located on the surface facing the large solvent channels. This observation suggests an inverse relation between solvent-reservoir size and radiation sensitivity of acidic residues on the reservoir surface.

(iii) Acidic residues stabilized by interactions with the side-chains of lysine and arginine residues, in particular those involved in complex salt-bridge clusters, are less radiation sensitive than those stabilized by interactions with the side-chains of serine, threonine and tyrosine residues. However, radiation damage does not seem to be related to the calculated pK_a values of acidic side-chains.

(iv) Radiation damage is not directly related to water accessibility.

References

Adam, V., Royant, A., Niviere, V., Molina-Heredia, F. P. & Bourgeois, D. (2004). *Structure*, **12**, 1729–1740.

Antosiewicz, J., McCammon, J. A. & Gilson, M. K. (1994). *J. Mol. Biol.* **238**, 415–436.

Baxter, R. H., Seagle, B. L., Ponomarenko, N. & Norris, J. R. (2004). *J. Am. Chem. Soc.* **126**, 16728–16729.

Birktoft, J. J. & Banaszak, L. J. (1983). *J. Biol. Chem.* **258**, 472–482.

Brünger, A. T., Adams, P. D., Clore, G. M., DeLano, W. L., Gros, P., Grosse-Kunstleve, R. W., Jiang, J.-S., Kuszewski, J., Nilges, N., Pannu, N. S., Read, R. J., Rice, L. M., Simonson, T. & Warren, G. L. (1998). *Acta Cryst.* D**54**, 905–921.

Burmeister, W. P. (2000). *Acta Cryst.* D**56**, 328–341.

Carugo, O. & Carugo, K. D. (2005). *Trends. Biochem. Sci.* **30**, 213–219.

Cendrin, F., Chroboczek, J., Zaccaï, G., Eisenberg, H. & Mevarech, M. (1993). *Biochemistry*, **32**, 4308–4313.

Clarke, A. R., Wilks, H. M., Barstow, D. A., Atkinson, T., Chia, W. N. & Holbrook, J. J. (1988). *Biochemistry*, **27**, 1617–1622.

Collaborative Computational Project, Number 4 (1994). *Acta Cryst.* D**50**, 760–763.

Costenaro, L., Zaccaï, G. & Ebel, C. (2001). *J. Cryst. Growth*, **232**, 102–113.

Dalhus, B., Saarinen, M., Sauer, U. H., Eklund, P., Johansson, K., Karlsson, A., Ramaswamy, S., Bjork, A., Synstad, B., Naterstad, K., Sirevag, R. & Eklund, H. (2002). *J. Mol. Biol.* **318**, 707–721.

Dean, R. T., Wolff, S. P. & McElligott, M. A. (1989). *Free Radic. Res. Commun.* **7**, 97–103.

DeLano, W. (2003). *The PyMOL Molecular Graphics System.* DeLano Scientific LLC, San Carlos, CA, USA.

Dubnovitsky, A. P., Ravelli, R. B., Popov, A. N. & Papageorgiou, A. C. (2005). *Protein Sci.* **6**, 1498–1507.

Dym, O., Mevarech, M. & Sussman, J. L. (1995). *Science*, **267**, 1344–1346.

Garman, E. (2003). *Curr. Opin. Struct. Biol.* **13**, 545–551.

Gerstein, M. & Chothia, C. (1991). *J. Mol. Biol.* **220**, 133–149.

Gilson, M. K. (1993). *Proteins Struct. Funct. Genet.* **15**, 266–282.

Heinig, M. & Frishman, D. (2004). *Nucl. Acid Res.* **32**, W500–502 (web server issue).

Henderson, R. (1990). *Proc. R. Soc. London Ser. B*, **241**, 6–8.

Irimia, A., Ebel, C., Madern, D., Richard, S. B., Cosenza, L. W., Zaccaï, G. & Vellieux, F. M. D. (2003). *J. Mol. Biol.* **326**, 859–873.

Irimia, A., Vellieux, F. M., Madern, D., Zaccai, G., Karshikoff, A., Tibbelin, G., Ladenstein, R., Lien, T. & Birkeland, N. K. (2004). *J. Mol. Biol.* **335**, 343–356.

Iwata, S., Kamata, K., Yoshida, S., Minowa, T. & Ohta, T. (1994). *Nature Struct. Biol.* **1**, 176–185.

Jones, T. A., Zou, J. Y., Cowan, S. W. & Kjeldgaard, M. (1991). *Acta Cryst.* A**47**, 110–119.

Kort, R., Hellingwerf, K. J. & Ravelli, R. B. (2004). *J. Biol. Chem.* **279**, 26417–26424.

Laskowski, R. A., MacArthur, M. W., Moss, D. S. & Thornton, J. M. (1993). *J. Appl. Cryst.* **26**, 283–291.

Lee, B. I., Chang, C., Cho, S. J., Eom, S. H., Kim, K. K., Yu, Y. G. & Suh, S. W. (2001). *J. Mol. Biol.* **307**, 1351–1362.

Leiros, H. K., Timmins, J., Ravelli, R. B. & McSweeney, S. M. (2006). *Acta Cryst.* D**62**, 125–132.

Leslie, A. G. W. (1992). *Joint CCP4 and ESF-EACMB Newsletter on Protein Crystallography*, Vol. 26. Daresbury Laboratory, Warrington, UK.

McClendon, S., Zhadin, N. & Callender, R. (2005). *Biophys. J.* **89**, 2024–2032.

Madern, D. (2002). *J. Mol. Evol.* **54**, 825–840.

Madern, D., Ebel, C. & Zaccaï, G. (2000). *Extremophiles*, **4**, 91–98.

Madern, D., Pfister, C. & Zaccaï, G. (1995). *Eur. J. Biochem.* **230**, 1088–1095.

Matsui, Y., Sakai, K., Murakami, M., Shiro, Y., Adachi, S., Okumura, H. & Kouyama, T. (2002). *J. Mol. Biol.* **324**, 469–481.

Mevarech, M., Frolow, F. & Gloss, L. M. (2000). *Biophys. Chem.* **86**, 155–164.

Murray, J. W., Garman, E. F. & Ravelli, R. B. (2004). *J. Appl. Cryst.* **37**, 513–522.

Murray, J. W., Rudino-Pinera, E., Owen, R. L., Griñinger, M., Ravelli, R. B. G. & Garman, E. F. (2005). *J. Synchrotron Rad.* **12**, 268–275.

Owen, R. L., Rudino-Pinera, E. & Garman, E. F. (2006). *Proc. Natl. Acad. Sci. USA*, **103**, 4912–4917.

Ravelli, R. B. & McSweeney, S. (2000). *Structure*, **8**, 315–328.

Richard, S. B., Madern, D., Garcin, E. & Zaccaï, G. (2000). *Biochemistry*, **39**, 992–1000.

Richard, S., Bonnete, F., Dym, O. & Zaccaï, G. (1995). *In Archaea: A Laboratory Manual*, edited by S. Dassarma, pp. 149–153. Plainview, NY: Cold Spring Harbor Laboratory Press.

Roberts, B. R., Wood, Z. A., Jonsson, T. J., Poole, L. B. & Karplus, P. A. (2005). *Protein Sci.* **14**, 2414–2420.

Tsou, C. L. (1998). *Biochemistry (Mosc.)*, **63**, 253–258.

Uchida, K. & Kawakishi, S. (1993). *FEBS Lett.* **332**, 208–210.

Vriend, G. (1990). *J. Mol. Graph.* **8**, 52–56.

Weik, M., Ravelli, R. B., Kryger, G., McSweeney, S., Raves, M. L., Harel, M., Gros, P., Silman, I., Kroon, J. & Sussman, J. L. (2000). *Proc. Natl. Acad. Sci. USA*, **97**, 623–628.

Weik, M., Ravelli, R. B., Silman, I., Sussman, J. L., Gros, P. & Kroon, J. (2001). *Protein Sci.* **10**, 1953–1961.

Yamada, Y., Fujiwara, T., Sato, T., Igarashi, N. & Tanaka, N. (2002). *Nature Struct. Biol.* **9**, 691–695.